

'Sling effect' in the development of atmospheric cascades induced by primary cosmic ray nuclei

¹ A.D.Erlykin ^(1,2), A.W.Wolfendale⁽²⁾

(1) *P. N. Lebedev Physical Institute, Moscow, Russia*

(2) *Department of Physics, University of Durham, Durham, UK*

Abstract

The 'Sling effect' appears when a fragment of a projectile nucleus emitted after its peripheral collision with a target nucleus is caused to rotate with high spin. The spinning fragment has a deformed shape and looks like an oblate ellipsoid. Due to the virtual non-compressibility of nuclear matter, and the polarization of the spin in the plane transverse to the input momentum of the projectile nucleus, such an ellipsoid has a reduced mean interaction cross-section compared with a non-spinning fragment which has a spherical shape. Purely geometrical arguments dictate that such an ellipsoidal nucleus should have additional fluctuations of cross-section even at a fixed impact parameter dependent on the orientation angle between the axis of the ellipsoid and the vector connecting the centers of the projectile and target nucleus. The number of 'wounded nucleons' in the projectile nucleus participating in the interaction correlates strongly with the interaction cross-section. All these effects lead to a non-exponential attenuation of fragments and an increased probability for a fragment to penetrate down to a larger depth in the absorber, than normal.

If the sling effect appears in the interaction of a primary cosmic ray nucleus with nuclei in the atmosphere the induced atmospheric cascade will have a slower attenuation, and thereby can help to reduce some important inconsistencies in the interpretation of the existing experimental data on extensive air showers observed in the lower half of the atmosphere. The paper gives numerical estimates of the sling effect.

1 Introduction

Information about nuclear interactions at energies higher than 2 PeV comes only from cosmic rays, viz. from the study of atmospheric cascades initiated by primary cosmic ray protons and heavier nuclei. Due to the largely unknown mass composition of the primary cosmic rays the only criterium of the correctness of the chosen interaction model, the mass composition and the adopted method of analysis, is the consistency of the results on the primary mass composition derived from different observables. A 'big leap' forward in this direction has been made with the development of the CORSIKA code for the simulation of

¹E-mail address: a.d.erlykin@durham.ac.uk

extensive air showers (EAS) which can incorporate and test different interaction models [1]. Using the results obtained with CORSIKA it was shown that the QGSJET model gives in general the most consistent description of the observed EAS characteristics and the mass composition [2, 3].

However, deeper analysis of the EAS data collected by the KASCADE experiment reveals that some serious inconsistencies still remain [4, 5]. There is a difference in the mass composition derived from observables which either include or ignore N_e - the electron size of the shower, as well as between results obtained from the ground-based measurements and from the distribution of X_{max} - the depth of the shower maximum in the atmosphere measured by means of Cherenkov light, etc. There have been different attempts to overcome these inconsistencies [6, 7]. All of them agree that the atmospheric cascade should be made more penetrative and propose different mechanisms for that. We have also examined this problem and come to the conclusion that the best way is to invoke a minor increase of the energy fraction transferred to the electromagnetic component ($K_\gamma = 0.26$) with *an increase of the 'elongation rate'* (the change in depth of maximum per decade of energy); the value needed is about 71 gcm^{-2} . Both modifications are easier to associate with nucleus-nucleus (AA) interactions than with (PA) collisions [8]. In the present paper we proceed further in this direction.

2 Slingshot effect

2.1 Fragmentation of the high energy nucleus

There is a vast literature on different aspects of AA - interactions. Important for our subject is the fact that complete fragmentation of a projectile nucleus does not occur at relativistic energies i.e. the nucleus is not split into independent nucleons. The general feature of the independence of the fragmentation process on the collision energy which is observed at energies above 20-30 GeV is known as *limiting fragmentation* [9, 10]. Some authors claim that the yield of heavy fragments even rises with energy up to 200 GeV/nucleon due to an increasing role of the electromagnetic excitation and dissociation of projectile nuclei [11]. For instance, in the interactions of Fe group nuclei ($22 < Z < 28$) with nuclear emulsions at 20-65 GeV/nucleon such a heavy fragment as Sc ($Z=21$) has been observed, amongst others [12]. Electromagnetic nuclear excitation and multifragmentation is observed in ultra-peripheral collisions even at RHIC energies ($\sqrt{s} = 200 \text{ GeV/nucleon}$, which corresponds to an equivalent energy of 4.3 PeV for gold in the laboratory coordinate system [13]) and used as a collider luminosity monitor [15]. In what follows we postulate that the process of nuclear fragmentation persists up to PeV energies in AA-interactions.

2.2 Rotation, polarization and deformation of the fragment

Nuclear fragments arising in grazing peripheral collisions at sub-GeV energies often rotate like a '*slingshot*' and achieve a high spin. This spin is polarized in the plane transverse to

the momentum of the projectile nucleus [16]. The effect is used at low and intermediate energies for the formation of polarized beams of low intensity [17]. In spite of the fact that the nuclear fragment is a composite, and often excited, object it demonstrates the features of collective motion and behaves like a liquid drop. Some features of collective motion of nuclear matter, eg the directed and elliptic flows and high transverse momenta of the fragments, are preserved even at relativistic energies [13, 14]. In this connection we assume that the features of the fragment's rotation and polarization persist at least up to PeV energies. An indirect indication that this assumption can be true is the alignment of energetic sub-cascades in multicore gamma-families detected by X-ray emulsion chambers at mountain altitudes and in the stratosphere [18]. Such alignment can be expected when the excited and spinning nuclear fragment decays and emits high energy particles preferentially in its rotation plane, like splashes from a rotating wheel or sparks from a grindstone [19].

Although the liquid drop model is not able to give a quantitative explanation of such fine features as gamma-ray spectra of excited nuclei, it is still useful for the modeling of the gross features, such as the shape of the excited nucleus, fluctuations of the collisional cross-section, the number of wounded nucleons etc (see §3). The use of more sophisticated quantum-mechanical models such as the shell model can reveal some tiny effects, but for our purposes of a semi-quantative classical consideration the use of the liquid drop model is sufficient.

Due to the rotation of the object with liquid drop properties its shape is deformed. In the classical consideration this deformation is caused by centrifugal forces, in the quantum mechanics the deformation is attributed to the state with a high angular momentum. The spherical fragment becomes an oblate spheroid with a shorter axis coincident with the axis of the spin. Following [20] we call the effect of the rotation, polarization and deformation of a nuclear fragment the '*sling effect*'. In the experimental study of deformed nuclei, spins of up to a few tens and deformations of nuclear sizes up to $\sim 30\%$ have been observed [21, 22].

3 A geometrical approach

3.1 General Remarks

Many features of AA-interactions are considered within a purely geometrical approach. The popular Bradt-Peters formula for the interaction cross-section of two nuclei [23] is just the result of the geometrical examination of the collision between two spheroids. The formulae for the mean number of wounded nucleons in colliding nuclei were also derived using geometrical arguments [24, 25]. We continue our consideration using the same geometrical approach. As an example, we consider the collision of an iron nucleus ^{56}Fe , which is one of major constituents of cosmic rays at the energies in question here, with a nitrogen nucleus ^{14}N of the Earth's atmosphere. As a result of this collision the fragment ^{45}Sc emerges and the remaining 11 nucleons are liberated from the parent iron nucleus with, on average, 8 being 'wounded'.

Some remarks are necessary also about cross-sections for nucleus-nucleus collisions. In the (assumed) absence of coherent effects and 'shadowing' phenomena, the number of nucleon-nucleon collisions will be independent of the manner in which the nucleons are packed, or distributed; thus, although the mean cross-section for nucleus-nucleus interaction will depend on the shape of the nucleus the product of cross-section and number of 'wounded' nucleons will be a constant. However, the magnitude of the fluctuations about the mean will depend on the manner of distribution. Clearly for the situation where the fluctuations are large there is the possibility of misidentification of the primary mass depending on whether the cross-section is high (high mass) or low (great penetration and therefore light mass). The latter situation is of great importance here.

3.2 The reduction of the mean cross-section

Returning to the interaction of an iron nucleus with a nitrogen nucleus and an emerging Sc fragment we assume that it moves down in the vertical direction and is subject to the 'sling effect'. This means that it rotates and has an ellipsoidal shape with a shorter axis orientated in the horizontal direction. Let us denote its longer axis as 'a' and the shorter axis as 'c'. The deformation of the spheroid is often characterized by an ellipticity ϵ , which is defined as $\epsilon = \sqrt{1 - c^2/a^2}$. Due to the non-compressibility of nuclear matter the volume of the deformed fragment should be equal to the volume of the spherical one, i.e. $\frac{4}{3}\pi a^2 c = \frac{4}{3}\pi R^3$, where R is the radius of the spherical fragment. Combining the formulae for ϵ and for the volume we obtain $a = R/(1 - \epsilon^2)^{1/6}$, $c = R(1 - \epsilon^2)^{1/3}$. If the ellipsoidal fragment moves down and its shorter axis is orientated horizontally then its geometrical cross-section seen 'edge-on' from below is πac . It means that this cross-section is equal to $\pi R^2(1 - \epsilon^2)^{1/6}$, i.e. reduced compared with a spherical fragment by the same factor of $(1 - \epsilon^2)^{1/6}$ as the increase of the longer axis.

The prolate configuration of the spheroid in which the spin is oriented along the longer axis 'a' if it exists in nuclear collisions should have an opposite effect, increasing the mean cross-section, but we consider it unlikely due to the effect of centrifugal forces. In both cases the surface of the deformed fragment has to increase with the rising ellipticity by 0.4% for $\epsilon = 0.5$ and by 14% for $\epsilon = 0.9$, but the volume according to our assumption remains constant.

In what follows we examine two cases with $\epsilon = 0.5$ and 0.9. The latter corresponds to the increase of the larger axis by about 32% and to the reduction of the shorter axis by 43%, which approximately corresponds to the magnitude of the deformation observed in experiments hitherto. For these values of ϵ the reduction of the purely geometrical cross-section is 5% and 24% respectively, which definitely should reduce the mean interaction cross-section between this fragment and the target nitrogen nucleus. The maximum observed hyperdeformation [22] in which the ratio of a long to a short radius achieved 3:1 corresponds to an ellipticity $\epsilon \approx 0.94$. At the end of the paper we examine the hypothetical case of $\epsilon = 0.99$ to show the rise of the sling effect if the nuclear deformation grows with energy.

In order to estimate the reduction of the cross-section we introduce the so called

collisional cross-section σ as a parameter for a single collision. It is equal to the overlap area between two colliding objects (Figure 1). In the case of the two spherical objects

COLLISION OF SPHERICAL AND ELLIPSOIDAL NUCLEI

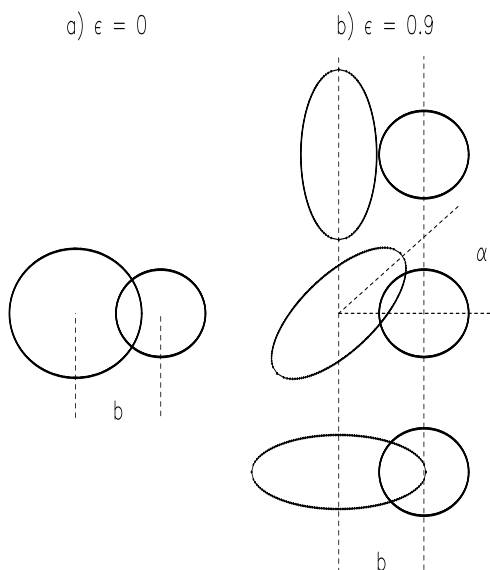


Figure 1: A schematic view of the collision: a) between two spherical nuclei and b) between an ellipsoidal fragment and spherical target, the impact parameter being the same in the two cases. It is seen that the overlap area in the latter case depends on the orientation angle α between the larger axis of the ellipsoid and the vector connecting the centers of the two nuclei even for a fixed impact parameter b .

it depends just on the radii of the objects R, r and the impact parameter b . In the case of the colliding ellipsoid and spheroid the overlap area depends not only on a, c, r and b , but also on the orientation angle α between the longer axis of the ellipsoid and the vector connecting the centers of the two objects [16] (see Figure 1). We have calculated this dependence for colliding nuclei of ^{45}Sc with $\epsilon = 0, 0.5$ and 0.9 and ^{14}N . The result of the integration of the overlap area over the impact parameter b as a function of the orientation angle α is shown in Figure 2. For simplicity the radii of non-deformed Sc and N nuclei have been taken as $R, fm = 1.2 \cdot A^{1/3}$, where A is the mass of the nucleus and the interaction occurred in every case when the overlap area was non-zero. It is seen that the dependence of the cross-section on α and the reduction of its mean value compared with the case of the non-deformed fragment with $\epsilon = 0$ becomes stronger with an increase of the ellipticity.

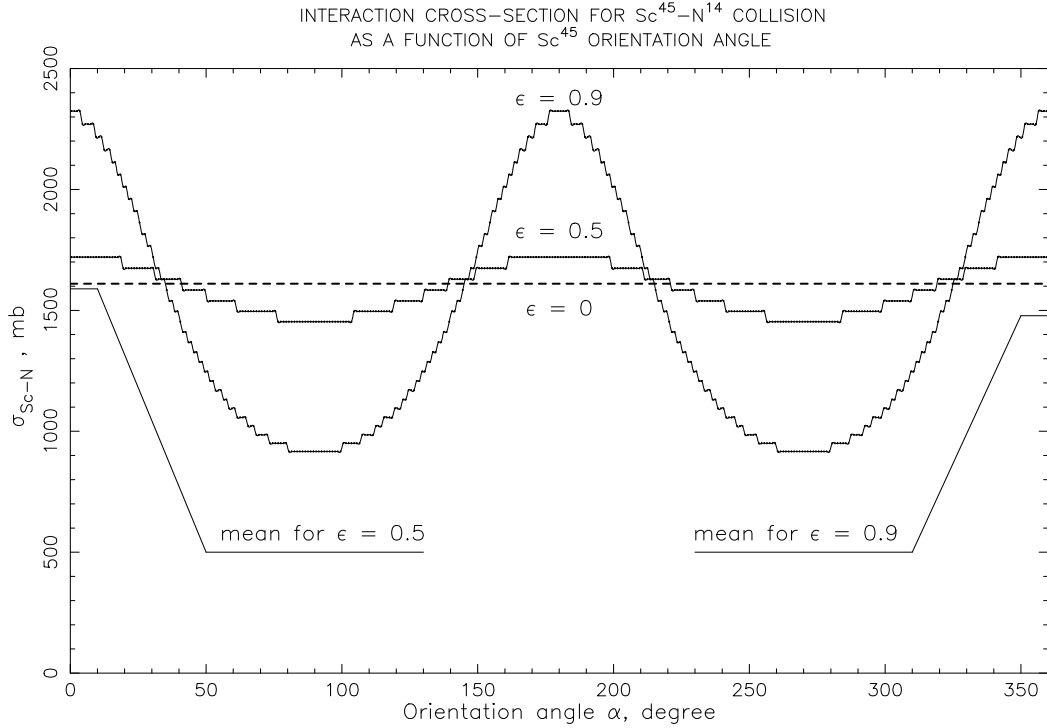


Figure 2: The interaction cross-section for $^{45}Sc - ^{14}N$ collision as a function of ^{45}Sc orientation angle α for the ellipticity $\epsilon = 0$ (dashed line), 0.5 and 0.9 (indicated in the Figure). The mean values of the cross-section averaged over the uniform distribution of α are also indicated for $\epsilon = 0.5$ and 0.9. The reduction of the mean cross-section for a deformed fragment of Sc with respect to a spherical one with $\epsilon = 0$ is clearly seen.

3.3 The attenuation of the deformed fragment

When the collisional cross section fluctuates, the interaction rate of the fragment changes and becomes non-exponential. We calculate it as

$$\frac{dP}{dz} = \int_0^{\infty} \sigma \exp(-\sigma z) \frac{dP}{d\sigma} d\sigma \quad (1)$$

where P is the probability for either the fragment to interact at the depth z , in the expression for $\frac{dP}{dz}$, or to collide with a cross-section σ in the expression for $\frac{dP}{d\sigma}$. We used a gaussian approximation of the $\sigma(\alpha)$ function in the range of $\alpha = 0^\circ - 90^\circ$ and the result of the integration compared with the interaction rate for the spherical fragment is shown in Figure 3. The non-exponential character of the interaction rate increases with ellipticity. It is seen that the ratio of interaction rates changes with atmospheric depth. The reduced rate at small depths leads to a higher probability for the fragment to penetrate deep into the atmosphere. It is the effect which we need in order to increase the penetrating ability of atmospheric cascades.

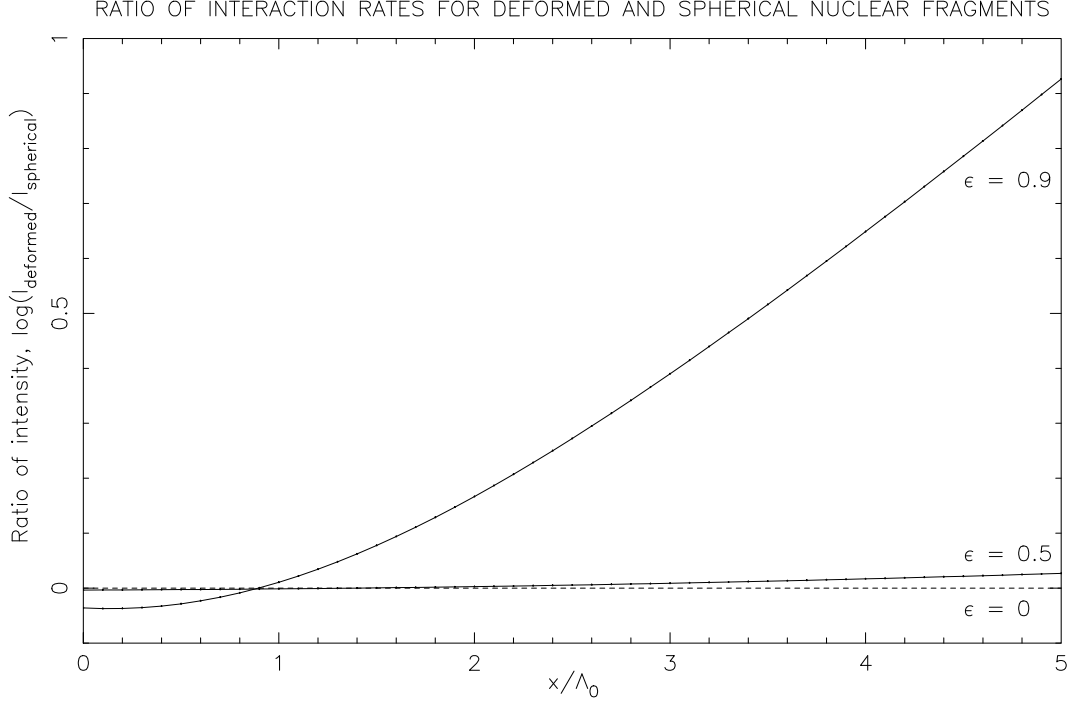


Figure 3: The ratio of the interaction rate for deformed ($\epsilon = 0.5$ and 0.9) and spherical ($\epsilon = 0$) Sc fragments in the air. Λ_0 is the mean interaction length of the spherical Sc fragment in the air. The reduced interaction rate at small depths leads to a reduced attenuation and to a higher probability of finding the fragment deep in the atmosphere.

3.4 The number of wounded nucleons

The attenuation of the atmospheric cascade induced by a nucleus is determined not only by the interaction rate of the fragment, but also by the number of nucleons participating in the interaction, which are usually called 'wounded nucleons'. The mean number of wounded nucleons and their fluctuations can be calculated using the Glauber approach, but, since it gives the same result [23] as the geometrical approach, we use the latter as more visual and simple. The meaning of the geometrical formulae used for the estimate of the mean number of wounded nucleons in the projectile nucleus **A** and in the target nucleus **B** can be seen from:

$$\begin{aligned}
 n_W^A &= A \frac{\bar{\sigma}_{pB}}{\bar{\sigma}_{AB}} = A \frac{S_B S_A}{\bar{\sigma}_{AB} S_A} = A \frac{S_{\text{overlap}}}{S_A} \\
 n_W^B &= B \frac{\bar{\sigma}_{pA}}{\bar{\sigma}_{AB}} = B \frac{S_A S_B}{\bar{\sigma}_{AB} S_B} = B \frac{S_{\text{overlap}}}{S_B}
 \end{aligned} \tag{2}$$

where n_W^A and n_W^B are the mean numbers of nucleons in the **A** or **B** nucleus uniformly distributed over its geometrical cross-section, which is cut by an overlap area of colliding nuclei. In the formula (2) $\bar{\sigma}_{pA}$, $\bar{\sigma}_{pB}$ and $\bar{\sigma}_{AB}$ are ordinary mean cross-sections for the

interaction of protons with **A** and **B** nuclei respectively and between **A** and **B** nuclei themselves, S_A, S_B are areas of **A** and **B** in the geometrical approach and $S_{overlap}$ is described below. In [26] we used this geometrical two-dimensional approach for the determination of the number of nucleons wounded in a *single* collision. In this case $S_{overlap}$ is the overlapping area which appears in one collision and can be different in another one. It depends on the ellipticity of the fragment ϵ , impact parameter b and orientation angle α .

In this paper we use a more accurate three-dimensional approach, taking

$$\begin{aligned} n_W^A &= A \frac{V_A^{overlap}}{V_A} \\ n_W^B &= B \frac{V_B^{overlap}}{V_B} \end{aligned} \quad (3)$$

where $V_A^{overlap}, V_B^{overlap}$ are the volume of the nucleus **A** and **B** respectively cut by the overlapping part of the counterpart nucleus (*tube*) and V_A, V_B are the total volumes of these nuclei. This approach, which could be called '*tube*' approach, implies that the nuclear density distribution inside the nucleus and therefore along the tube is uniform.

The dependence of n_w on α for $\epsilon = 0, 0.5$ and 0.9 for different fixed impact parameters b is shown in Figure 4a.

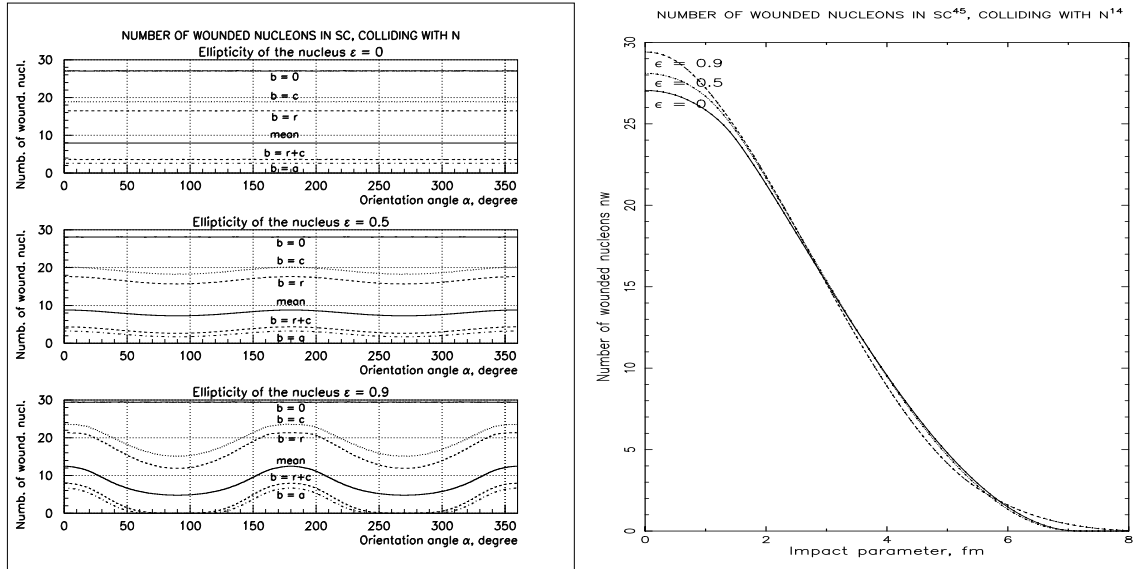


Figure 4: a) The dependence of the number of wounded nucleons n_w in a single collision on the orientation angle α for the ellipticity of the projectile fragment $\epsilon = 0, 0.5$ and 0.9 and for the fixed impact parameters $b = 0, r$ - the radius of target nucleus, c and a - small and large axes of the ellipsoid respectively, the sum $r+c$ and the mean $\langle n_w(\alpha) \rangle$ averaged over the impact parameter b . b) The dependence of the mean number of wounded nucleons $\langle n_w(b) \rangle$ on the impact parameter b averaged over the uniform distribution of orientation angles α .

It is seen that the dependence on α increases with the ellipticity ϵ . With an increased ellipticity the maximum impact parameter at which the interaction could occur increases too as well as the maximum length of the tube in the projectile nucleus. Due to this deformation and the constant nuclear density the range of the impact parameters and the maximum number of wounded nucleons increase too (Figure 4b).

3.5 The distribution of the number of wounded nucleons and its correlation with the cross-section

Due to the stochastic fluctuations of the impact parameters and orientation angles the number of wounded nucleons also fluctuates. Its distribution is shown in Figure 5a. It

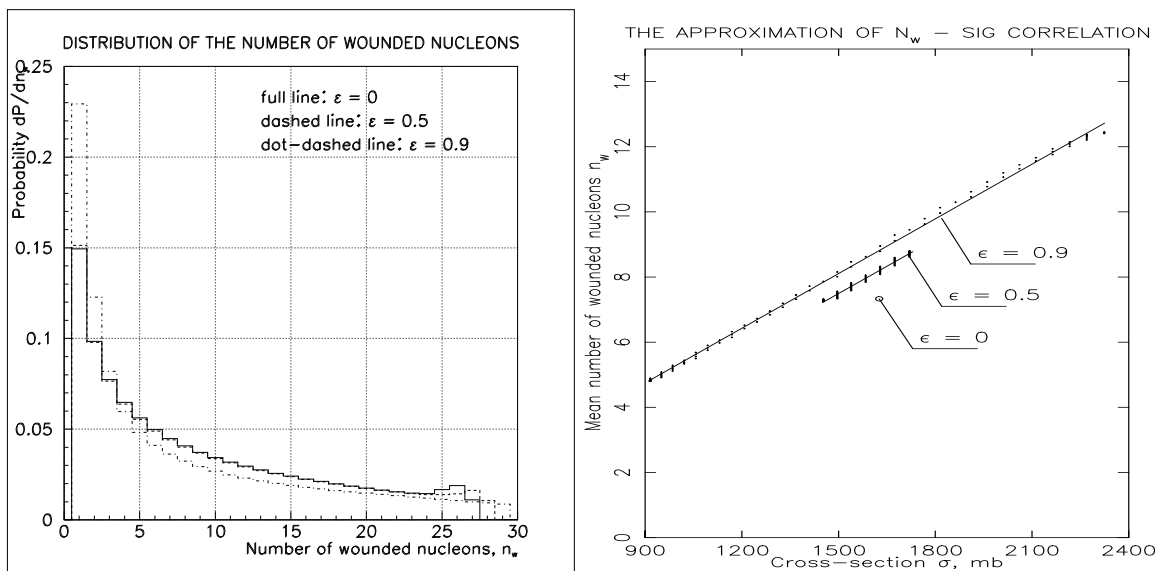


Figure 5: (a)-the distribution of the number of wounded nucleons and (b)-the correlation between the collisional cross-section and the number of wounded nucleons for the different ellipticity of the projectile fragment: $\epsilon = 0, 0.5$ and 0.9 . Lines are linear fits of the numerical data.

is seen that the width of the distribution increases with the ellipticity. An important consequence of the deformation is the strong correlation between the number of wounded nucleons and the collisional cross-section. It is an evident feature because n_w is strongly connected with the overlap area σ in the single collision. This correlation is shown in Figure 5b for n_w and σ averaged over all impact parameters. The existence of this correlation is a new feature for the interaction of deformed fragments and is important for their propagation through an absorber and the subsequent development of cascades initiated by high energy nuclei.

4 The longitudinal development of the nucleus-induced cascade

4.1 The longitudinal development of the nucleon component

In our example of the primary ^{56}Fe induced cascade we adopted the case where the interaction of the primary iron was normal with a deformed spinning ^{45}Sc fragment emitted. In the collision of the ^{45}Sc fragment with a nitrogen nucleus of the air on average 7 projectile nucleons were wounded and the other 38 nucleons of the fragment liberated as spectators and propagated through the atmosphere in an ordinary way. Therefore the difference between the longitudinal development of the nucleon component in an ordinary cascade and the cascade with a spinning fragment is determined by the greater penetrating ability of the fragment. We have calculated the interaction rate of nucleons in our Fe-induced cascade with a spinning Sc fragment and compared it with the nucleon interaction rate in the ordinary Fe-induced cascade. The result for the case of $\epsilon = 0.9$ is shown in Figure 6.

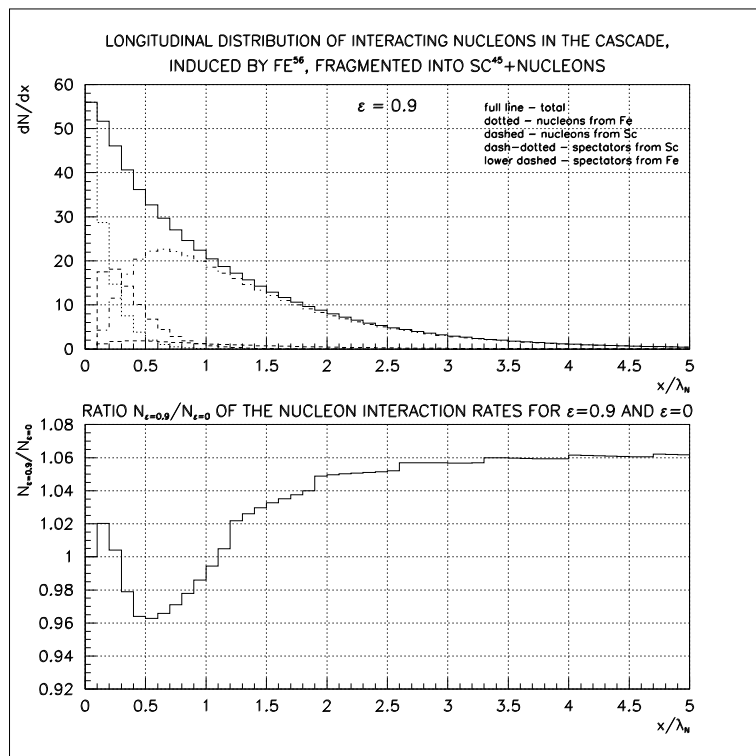


Figure 6: a) The interaction rate of nucleons in Fe-induced cascade: dotted line - wounded nucleons from Fe, dashed line - wounded nucleons from Sc, dash-dotted line - spectators from Sc, lower dashed line - spectators from Fe. b) The ratio of nucleon interaction rates in the cascade with a spinning Sc fragment and in an ordinary Fe-induced cascade with non-spinning Sc.

It is seen that in the cascade with a spinning fragment the interaction rate decreases

at the initial stages of the cascade development and on the contrary increases later - the effect which we needed to make the cascade able to penetrate deeper into the atmosphere, although the absolute value of the effect does not exceed a few percent even for $\epsilon = 0.9$. For $\epsilon = 0.5$ it is even less.

4.2 The longitudinal development of the Fe-induced cascade

In order to calculate the influence of the sling effect on the development of the electromagnetic component of EAS we used the approximate formulae for the cascades initiated by nucleons proposed in [27] and used by us in [8]. These formulae are results of the analytical solution of the system of kinetic equations for the development of the nucleon, pion and electromagnetic components of EAS [8]. Interaction rates of nucleons in the Fe-induced cascade were taken from the previous subsection. The result for a primary Fe nucleus of 1 PeV energy is shown in Figure 7. It is seen that the development of the

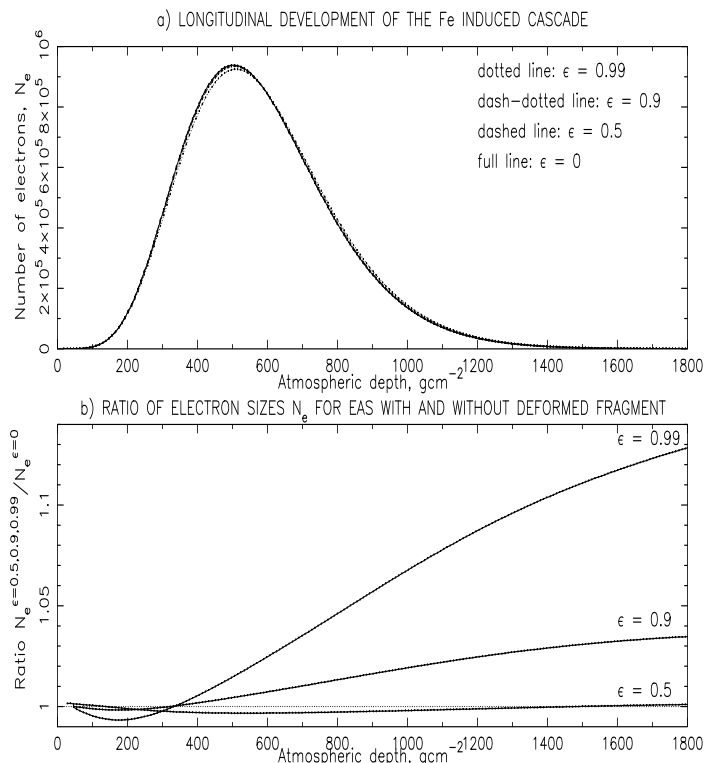


Figure 7: a) The longitudinal development of 1 PeV Fe-induced EAS with the emission of a Sc fragment with different ellipticity. The difference between $\epsilon = 0, 0.5$ and 0.9 is small and not seen at this graph. The difference between $\epsilon = 0.99$ and 0 is more pronounced: the cascade with a deformed fragment is shifted to a larger depth. b) The ratio of the shower size N_e for $\epsilon = 0.5, 0.9, 0.99$ and 0 as the function of the atmospheric depth.

electromagnetic component resembles that of the nucleon component, viz. the cascade develops later, its size at the early stages of the development is smaller, but larger at large

atmospheric depths. For moderate ellipticities, not exceeding 0.9, the magnitude of the sling effect is small, however. The shift of X_{max} - the maximum cascade development, does not exceed 1 gcm^{-2} . The increase of the size at sea level for $\epsilon = 0.9$ is about 2%.

4.3 The possible role of the sling effect at ultra-high energies

The sling effect becomes stronger when the smaller radius of the deformed fragment becomes comparable or even less than the radius of the target nucleus. In our example of colliding ^{45}Sc and ^{14}N it happens just when the ellipticity approaches 0.9. The maximum deformation observed hitherto corresponds to an ellipticity $\epsilon = 0.94$ [22]. However, these observations have been made at low energies. We have assumed that at higher energies the deformation can be even higher and calculated the longitudinal development of the Fe induced cascade for the hypothetical deformation of a Sc fragment equal to 0.99. It is also shown in Figure 7. The sling effect for this case is certainly greater. The shift of X_{max} increases up to 5 gcm^{-2} and the increase of the shower size at the sea level grows by up to 7%. Therefore the sling effect can be important if the deformation of fragments emitted in nucleus-nucleus collisions grows with energy beyond the values observed hitherto.

The elongation rate for nucleus-induced cascades will be, in this case, also higher than without the sling effect and the interpretation of experimental data on X_{max} distributions should be re-examined; the effect leads to a higher abundance of heavy nuclei in PeV cosmic rays. At the ultra-high energies ($\simeq 10^{20}$ eV) the effect can be very large and the consequences for the mass composition of the important extragalactic particles rather profound.

In particular, the substantial increase of fluctuations in the collisional cross-section and the number of wounded nucleons could be responsible, at least partly, for the seeming contradiction between the mean and the width of the X_{max} distribution in the stereo Fly's Eye measurements [28]. The mean $\langle X_{max} \rangle$ was even less than that expected for pure iron, but the fluctuations of X_{max} exceeded those expected for pure protons and corresponded rather to the mixed composition.

The relativistic expansion of the time needed for the formation of a stable rotation and deformation of the fragment cannot change the effect, since this time is about 10^{-22} sec in the fragment's rest system and even such Lorentz-factors as $\sim 10^{11}$ cannot make it comparable with the time needed to move between the collision in which this fragment has been produced, and its next collision, which is about 10^{-5} sec at high atmospheric altitudes.

5 Conclusions

We have examined the possible slowing down of the development of the atmospheric cascade initiated by a primary nucleus of high energy due to the 'sling effect', which is the rotation, deformation and polarization of nuclear fragments emitted in the nucleus-nucleus interactions. At the moment it is difficult to make accurate estimates of this

effect, because of lack of experimental data on the fragmentation of nuclei and on the excitation, polarization and interactions of the emitted nuclear fragments but we have made an attempt. In the examined example of the emission of just one ^{45}Sc fragment from the interaction of a 1 PeV primary ^{56}Fe nucleus, if the ellipticity of the fragment does not exceed 0.9, the effect is rather small. The shift of the cascade maximum does not exceed 1 gcm^{-2} and the increase of the shower size at sea level is about 2%. These changes alone are not sufficient to eliminate inconsistencies in the interpretation of experimental data on EAS discussed in the Introduction.

However, numerical values of the mass, multiplicity and ellipticity of the fragment in the examined example were taken from the experiments at GeV and TeV energies. If there is an energy dependence of these characteristics and the ellipticity rises with energy, as seems likely, the sling effect can be much stronger. For the hypothetical case of $\epsilon = 0.99$ the shift of X_{max} increases up to 5 gcm^{-2} and the shower size at the sea level grows up to 7%.

If this rise is real the role of the sling effect at ultra-high energies can be very important and should be taken into account in the models of nucleus-nucleus interactions. It can have a profound effect on the inferred primary mass - a quantity of considerable astrophysical significance.

Finally, attention can be given to the phenomenon of 'alignment'; this phenomenon has various interpretations [19, 20] and it would be promising to search for the sling effect in the azimuthal alignment of the secondary particles on the event by event basis directly in nucleus-nucleus interactions at RHIC and LHC.

Acknowledgments

We thank M.Baldo and G.I.Orlova for useful discussions, R.A.Mukhamedshin for sending us some unpublished materials and anonymous referees for critical remarks and suggestions. One of us (ADE) thanks The Royal Society for financial support.

References

- [1] Heck D. et al., 1998, FZKA Report Forschungszentrum Karlsruhe 6019
- [2] Erlykin A.D., Wolfendale A.W., 1998, *Astroparticle Physics*, **9**, 213
- [3] Antoni T. et al. 1999, *J.Phys.G: Nucl.Part.Phys.*, **25** , 2161
- [4] Roth M. et al. 2001, *Proc. 27th ICRC, Hamburg*, **1**, 88
- [5] Haungs A. et al. 2003, *Progr. Nucl. Part. Phys.*, **66**, 1145
- [6] Hörandel J.R. 2003, *J.Phys.G: Nucl.Part.Phys.*, **29**, 2439
- [7] Yakovlev V.I. 2003, *Nucl. Phys. B (Proc.Suppl.)*, **122**, 417

- [8] Erlykin A.D., Wolfendale A.W., 2002, *Astroparticle Physics*, **18**, 151
- [9] Adamovich M.I. et al., 1989, *Phys. Rev. Lett.*, **62**, 2801
- [10] Back B.B., 2003, *Phys. Rev. Lett.*, **91**, 052303
- [11] Waddington C.J. et al., 1990, *Proc. 21st ICRC, Adelaide*, **8**, 87
- [12] Burnett T. et al. 1987, *Phys. Rev.* **D35**, 824
- [13] Klein S.R., 2003, *Nucl. Phys. B (Proc.Suppl.)*, **122**, 76
- [14] Adamovich M.I. et al., 2004, *Physics of Atomic Nuclei*, **67**, 290
- [15] Adler C. et al. nucl-ex/0206004
- [16] Fick D., 1981, *Ann. Rev. Nucl. Part. Sci.*, **31**, 53
- [17] Satchler G.R., *Introduction to Nuclear Reactions*, Macmillan Press Ltd., New York, 1980
- [18] Capdevielle J.N. and Slavatinsky S.A., 1999, *Nucl. Phys. B (Proc. Suppl.)*, **75A**, 12
- [19] Mukhamedshin R.A., 2001, *Nucl. Phys.B (Proc.Suppl.)*, **97**, 122
- [20] Dremin I.M., Man'ko V.I. 1998, *Nuovo Cimento*, **111A**, 439
- [21] Royer G. and Haddad F., 1993, *Phys. Rev. C*, **47**, 1302
- [22] Lafosse D.R. et al., 1995, *Phys. Rev. Lett.*, **74**, 5186
- [23] Bradt H.L., Peters B., 1948, **74**, 1828
- [24] Bialas A. et al., 1976, *Nucl. Phys.* **B111**, 461
- [25] Shabelsky Yu.M., 1979, *Acta Phys. Polonica*, **B10**, 1049
- [26] Erlykin A.D., Wolfendale A.W., 2004, *Nucl. Phys. B (Proc.Suppl.)*, **136**, 282
- [27] Catalano O. et al, 2001, *Proc. 27th ICRC, Hamburg*, **2**, 498
- [28] Cassiday G.L. et al, 1990, *Astrophys. J.*, **356**, 669